On the origin of fatigue corrosion cracking in Al7075

Über den Ursprung von Schwingungsrisskorrosion in Al7075

R. Masendorf[1], S. Dahle[2,3], L. Wegewitz[2,3], S. Korte[3], G. Lilienkamp[3], F. Voigts[3,4], W. Maus-Friedrichs[2,3]

The fatigue corrosion cracking of the Al7075 alloy has been investigated by Scanning Electron Microscopy (SEM) and Auger Electron Spectroscopy (AES). Specimen exposed to cyclic load at room temperature until crack initiation show a significant increase of magnesium within a distance of about 1 μm around the crack, while almost no aluminum was left. This segregation effect has been investigated in detail, yielding that the diffusion should most likely be driven by the gradient of the chemical potential through the oxidation of magnesium at the surface, while the required mobility for the diffusion process was gained by the mechanical stress of the cyclic loading.

Keywords: Fatigue Corrosion Cracking / Crack initiation / Auger Electron Spectroscopy / Aluminium / Al7075

Die Schwingungsrisskorrosion der Aluminiumlegierung 7075 wurde mit Rasterelektronemikroskopie und Augerelektronenspektroskopie untersucht. Proben, die bei Raumtemperatur bis zur Rissbildung einer zyklischen Last ausgesetzt waren, zeigen eine signifikante Erhöhung des Magnesiumgehalts in der Umgebung um den Riss, während fast kein Aluminium übrig bleibt. Dieser Segregationseffekt wurde im Detail untersucht. Dabei ergibt sich, daß die Diffusion höchstwahrscheinlich vom Gradienten des chemischen Potenzials durch die Oxidation von Magnesium an der Oberfläche getrieben wird. Die nötige Mobilität für den Diffusionsprozess liefert die mechanische Spannung durch die zyklische Last.

Schlüsselwörter: Schwingungsrisskorrosion / Rissbildung / Augerelektronenspektroskopie / Aluminium / Al7075

1 Introduction

In a specimen subjected to a cyclic load, a fatigue crack nucleus can be initiated on a microscopical scale, followed by cracks growing to macroscopic size, finally leading to specimen failure. Fatigue life is usually split into a crack initiation period and a crack growth period. It is accepted, that extrusions and intrusions in slip bands are the reason for crack initiation at surfaces under cyclic load [11]. Another important aspect is the interaction with the environment. A slip step at the free surface implies that fresh material is exposed to the environment. In a non-inert environment, most technical materials are rapidly covered with a thin oxide layer, or chemisorption of atoms from the environment occurs. An exact reversibility of slip is then prevented [2]. The combined influence of cyclic load and corrosion on crack initiation and propagation is called fatigue corrosion cracking (FCC). The initiation period is supposed to include some microcrack growth, but the fatigue cracks are still too small to be visible. In the second period, the crack grows up to complete failure of the specimen [3]. Two sequential processes during crack propagation have been identified, namely water vapour adsorption on crack tip surfaces and hydrogen embrittlement of cyclically deformed material within the plastic zone. These phenomena account for environmentally-assisted fatigue crack propagations [4]. Whereas the period of crack growth has been frequently investigated, only little knowledge on the initiation period exists, even though this period can account for up to 90% of the fatigue life of mechanical components parts [5]. In the case of static load the stress corrosion cracking (SCC) has been shown to be dependent on precipitation of a magnesium-rich β phase (Al_3Mg_2) at grain boundaries of aluminium-magnesium alloys AA5083 [6]. This magnesium segregation leads to accelerated hydrogen enrichment and thus accelerated crack propagation in case of the aluminum alloy 7050 [7]. These processes require additional energy to achieve sufficient fast diffusion rates. Thermal treatment is one possible way to provide this energy, but also cyclic strain amplitudes might supply sufficient activation energy, i. e. during FCC. Since the cracking is affected through magnesium-enrichment after thermal annealing at less than 200 °C the energy supplied by cyclic stress load appears sufficient

[1] Institut für Maschinelle Anlagentechnik und Betriebsfestigkeit, Technische Universität Clausthal, Clausthal-Zellerfeld, Germany
[2] Clausthaler Zentrum für Materialtechnik, Technische Universität Clausthal, Clausthal-Zellerfeld, Germany
[3] Institut für Energieforschung und Physikalische Technologien, Technische Universität Clausthal, 38678 Clausthal-Zellerfeld, Germany
[4] Institut für Mechanische Verfahrenstechnik, Technische Universität Clausthal, Clausthal-Zellerfeld, Germany

Corresponding author: Prof. Dr. Wolfgang Maus-Friedrichs, TU Clausthal, IEPT, Leibnizstraße 4, 38678 Clausthal-Zellerfeld
E-mail: w.maus-friedrichs@pe.tu-clausthal.de

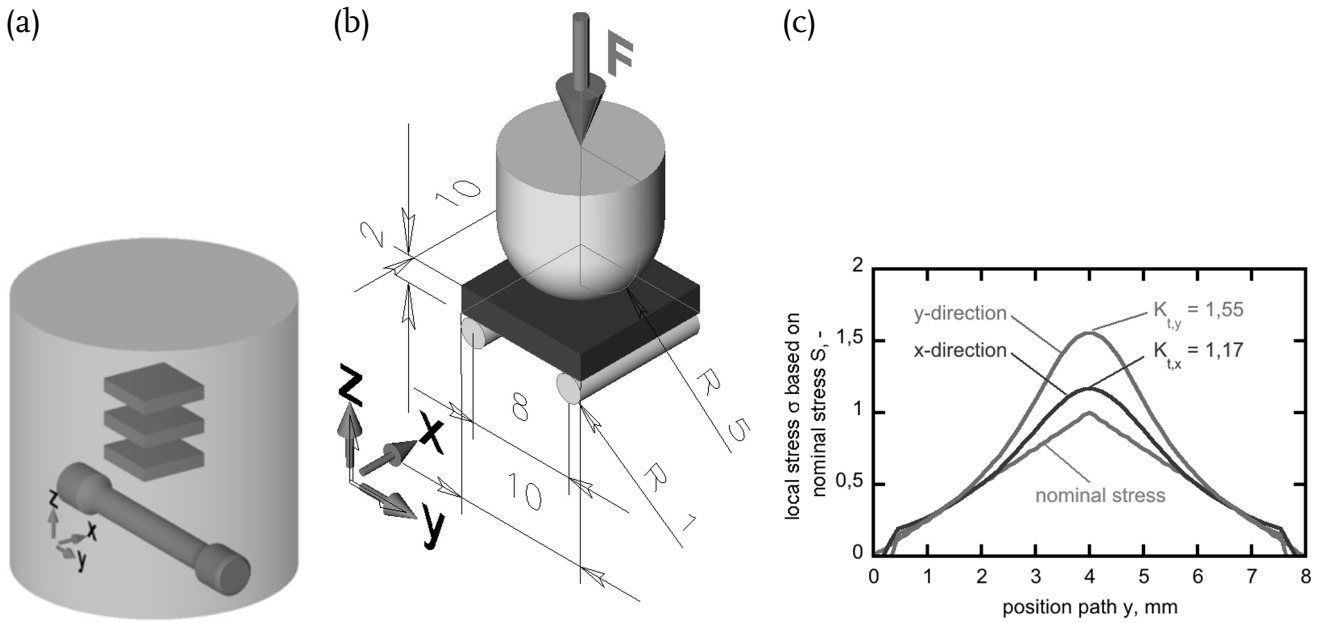

Figure 1. Schematic drawings of the specimen production and stress distrubtion: **(a)** specimen extraction from round Al7075-T6 bar (ø 40 mm), at the top fatigue specimens, at the bottom tensile test specimen (not used here), **(b)** specimen mount and specimen, blue = specimen, green = load application, **(c)** inhomogeneous stress distribution in the specimen due to punctual load application, local stress σ_x and σ_y in y-direction, half model.

Bild 1. Schematische Darstellung der Probenherstellung und Spannungsverteilung: **(a)** Probenherstellung aus einem runden Stab aus Al7075-T6 (ø 40 mm), oben Proben für die zyklische Belastung, unten Proben für Zugversuch (hier nicht verwendet), **(b)** Probe (blau) und Probenhalterung (grün), **(c)** inhomogene Spannungsverteilung in der Probe aufgrund der punktförmigen Belastung, lokale Spannung σ_x und σ_y in y-Richtung, Halbmodell.

Table 1. Composition of Al7075.

Tabelle 1. Zusammensetzung von Al7075.

element	Al	Zn	Mg	Cu	Fe	Si	Cr	Mn	Ti	other
mass-%	rest	5.10–6.10	2.10–2.90	1.20–2.00	0.50	0.40	0.18–0.28	0.30	0.20	0.15
at.-%	rest	2.19–2.62	2.43–3.36	0.53–0.88	0.25	0.40	0.10–0.15	0.15	0.12	0.10

for the activation of magnesium transport [8, 9]. Whereas the crack propagation and its relation to magnesium diffusion have been investigated for some time, no investigations on the effect of magnesium on the crack initiation has been published until now [6, 10–17].

The modifications of the specimen composition during crack initiation were investigated in the case of cyclic load applied to flat, notch-free specimen by applying Scanning Auger electron Microscopy (SAM). The use of Auger electrons excited by a well focused electron beam combines chemical information for all elements heavier than Lithium with a high spatial resolution. Auger electron energies are element specific and give a certain indication of the chemical environment of detected elements providing discrimination between e.g. metallic and oxidized aluminum and magnesium [18, 19]. The fraction of the specimen which accounts for the Auger signal has a lateral extension which is mainly determined by the diameter of the primary electron beam. Perpendicular to the surface it is limited by the energy dependent mean free path of the Auger electrons which is for example about 1.2 nm for a kinetic energy of 1000 eV. Thus, the volume probed in SAM is up to five orders of magnitude smaller than for X-ray fluorescence techniques such as EDX. In combination with ion sputtering elemental depth profiles with a resolution of a few atomic layers can be recorded. This is extremely important for segregation processes at surfaces. Results are presented for the aluminum alloy 7075-T6.

2 Experimental

2.1 Configuration of the test bench

Square, flat specimens ($10 \times 10 \times 2$ mm³) were machined from a round bar of 7075-T6 aluminum with the chemical composition given in *Tab. 1* in a manner depicted in *Fig. 1*a [20, 21]. The specimens' lower side is rested on two line supports 8 mm apart. The punctual test load is applied to the upper side of the specimen using a hemispherically shaped stamp, Fig. 1b. Due to the point-shaped load application an inhomogeneous stress distribution

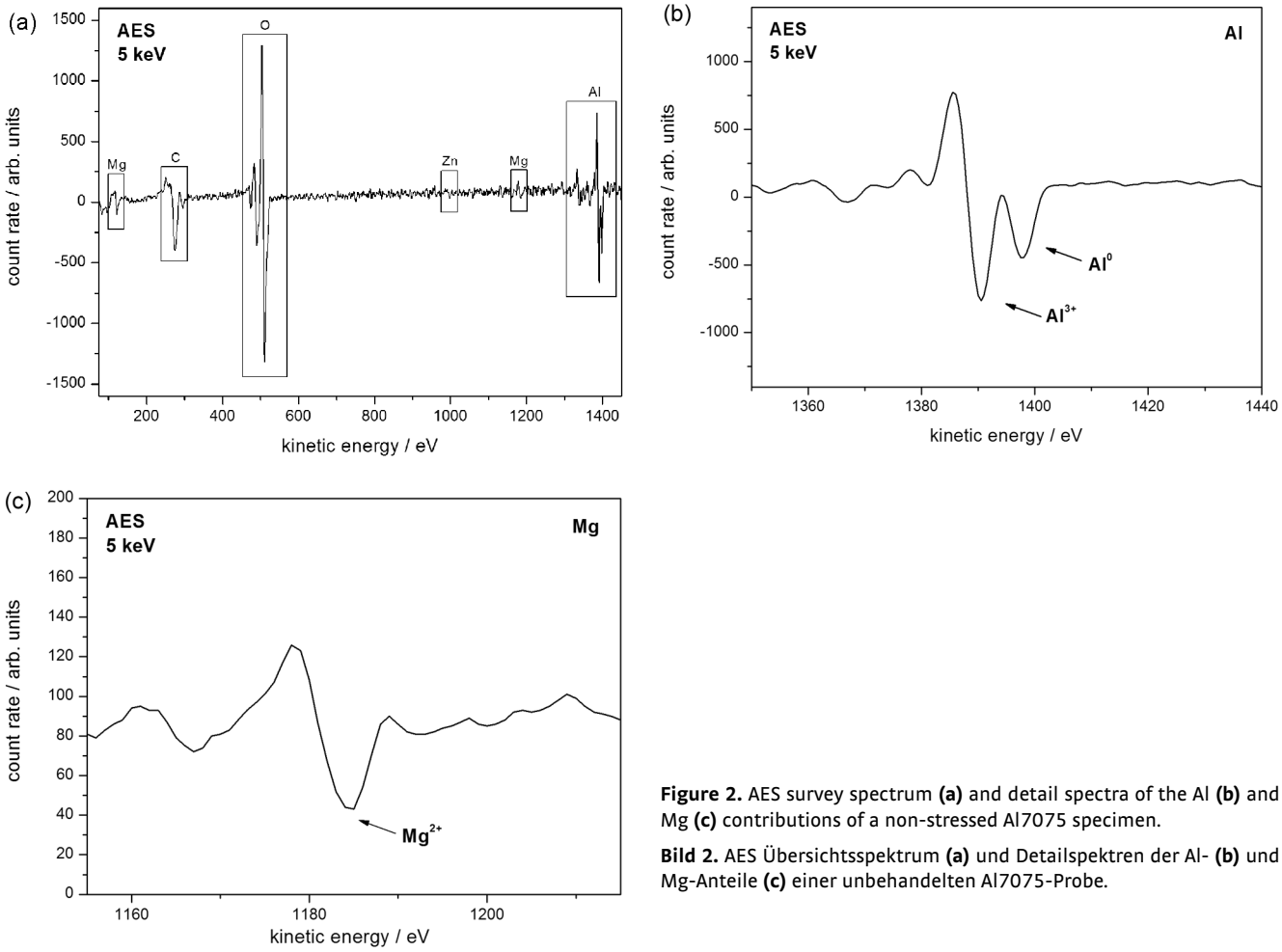

Figure 2. AES survey spectrum **(a)** and detail spectra of the Al **(b)** and Mg **(c)** contributions of a non-stressed Al7075 specimen.

Bild 2. AES Übersichtsspektrum **(a)** und Detailspektren der Al- **(b)** und Mg-Anteile **(c)** einer unbehandelten Al7075-Probe.

arises, which is calculated by a Finite Elemental Method (FEM). Compared to the theoretical mean stress for bar-shaped geometries $S_{b,\max}$ the local stress $\sigma_{b,\max}$ is raised. The resulting notch factor is defined by

$$K_t = \frac{\sigma_{b,\max}}{S_{b,\max}}$$

The progression of stress along a path on the underside of the specimen shows the elevation of stress in the center of the specimen, Fig. 1c. For the most stressed point in the center of the specimen, two direction dependent notch factors can be determined:

y-direction: $K_{t,y} = 1.55$

x-direction: $K_{t,x} = 1.17$

The fatigue testing loads are generated on an electromagnetical resonance testing machine at atmosphere. The excitation is applied with a resonance frequency which depends on the stiffness of the combination specimen-testing machine. In this case a testing frequency of around 60 Hz was applied. Any fracturing of the specimen leads to a loss of resonance system stiffness, the resonance frequency of the whole system falls off. This falloff is used to terminate the test. A frequency drop of 1 Hz corresponds to a crack length of roughly 3 mm on the surface of the specimen.

After fatigue testing the specimen is removed from the machine and the crack surfaces are analyzed.

2.2 Microscopy and Spectroscopy

A scanning Auger electron microscope (Omicron NanoSAM) with a base pressure below 10^{-10} mbar is used for spectroscopic and microscopic investigations [22]. Scanning Electron Microscopy (SEM) is applied to image details of the crack and determine the spot positions for Auger Electron Spectroscopy (AES) measurements. The beam current during operation was 1.5 nA at a primary electron energy of 5 keV and a spot size diameter of 3–5 nm. Thin surface layers can be removed by Ar^+ ion sputtering. This allows for Depth Profile Analysis (DPA) by alternating sputter cycles and Auger analysis. The focused Ar^+ ion beam is scanned across an area of about $1400 \times 1400\ \mu m^2$ to achieve a homogenous abrasion in the investigated area during depth profiling. This procedure enables access to the stoichiometry as a function of depth. The vertical resolution is merely limited by the mean free path of the Auger electrons and disorder introduced by ion bombardement such as roughening and mixing [23]. To calculate the sputter depths from the known sputter times a conversion factor for oxidic systems based on SiO_2 references is applied (1 nm depth corresponds to a sputter time of 40 s). The

sputter rate for pure Al_2O_3 is about 0.46 times lower [24]. Thus, 1 nm Al_2O_3 is removed after 87 s with our ion gun system. As the composition of the examined structures is strongly dependent on the depth below the surface it is not possible to figure out a correct calibration factor to convert sputter times to depth. For the oxidized top layer the correspondence of a sputter time of 87 s to 1 nm which is valid for Al_2O_3 may serve here as an approximate value.

3 Results

In *Fig. 2*a an Auger survey spectrum of the unstressed Al7075 specimen after polishing is shown. The differentiated Auger amplitude $\frac{dN}{dE}$ is displayed as a function of kinetic energy E of the emitted electrons. Besides aluminum, magnesium and zinc as metallic alloying constituents are detected. Furthermore, oxygen from the oxidized metallic surface and as part of surface contaminations such as carbonates is detected. The oxygen concentration, however, is far below the value for stoichiometric aluminum and magnesium oxides. The large amount of carbon is mainly due to surface contaminations.

More chemical information can be obtained from the detail spectra in Fig. 2b and 2c. In Fig. 2b the higher energetic aluminium peak at 1396 eV (minimum position) can be attributed to metallic aluminum from the specimens bulk. It is covered by a native oxide layer which is responsible for the energetically lower aluminium Auger transition at about 1390 eV. This chemical shift is typical of native oxide layers. For comparison: the shift in stoichiometric alumina with respect to metallic aluminum is about 16 eV.

Fig. 2c shows details of the magnesium spectrum. Even though single crystalline magnesia has a larger chemical shift than observed here, the peak shape indicates that the detected magnesium is in an oxidized state. The reasons for the small chemical shift compared to the well ordered oxides may be caused by the disordered oxide layer, understoichiometric oxygen concentration and the integration of carbon into the oxide layer.

Carbon can be detected throughout the whole oxide layer. The oxide film thickness on aluminium and Al7075 surfaces were previously determined to be about 2.1 nm on the basis of XPS studies for in vacuo oxidized specimens and about 4 nm maximum for atmospheric oxidation [25]. The mean free path of aluminium Auger electrons with nearly 1400 eV energy is about 2 nm. Thus, our Auger data, where metallic aluminum is visible through the native oxide layer, suggest an oxide thickness of about 2 nm. Besides the carbon contamination, a substoichiometric oxygen concentration and a doubled magnesium concentration (7.6 at.-% of the metals in the alloy, i. e. without considering oxygen and carbon) in comparison to the nominal value was found.

An Al7075 specimen with same composition has been exposed to mechanical stress in a resonance testing apparatus as described in chapter 2. A fatigue crack has been initiated in the center of the specimen where the maximum strain occurs under biaxial stress, according to our FEM analyses.

Fig. 3 shows a SEM image of this crack taken with an in-lens detector under 30° impact angle. On the right side of the figure

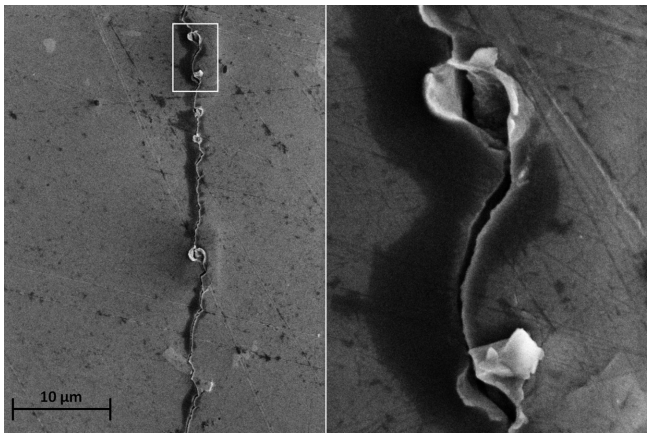

Figure 3. SEM image showing a typical part of the crack on a stressed Al7075 specimen; for details of the mechanical handling see text.

Bild 3. Rasterelektronenmikroskopische Aufnahme eines typischen Teils des Risses auf einer zyklisch belasteten Al7075-Probe; siehe Text für die Details der mechanischen Behandlung.

an enlarged image of the area marked by the white rectangle is shown. The bright features peeled off during crack formation, their contrast is mainly determined by topography. With the exception of a few spots the crack is surrounded by a dark rim. The darker color might be due to chemical contrast which is one of the dominant contrast mechanisms when using SEM in-lens detectors. Accordingly, Auger electron microscopy has been performed to investigate the spatially resolved composition of the specimen.

*Fig. 4*a shows an Auger survey spectrum taken at a primary energy of 5 keV during scanning the beam in a reduced raster of 145×175 nm^2 size placed in the darker rim close to the crack. The main constituents are magnesium, carbon and oxygen. Surprisingly, the aluminum signal is in the range of the noise level. Following the arguments given with Fig. 2c for the magnesium peak, magnesium is found to be completely non-metallic, again. After sputtering with 4 keV Ar^+ ions for 20 s, which is enough to remove the surface contamination due to adsorption in atmosphere further Auger spectra were recorded, Fig. 4b and Fig. 4c. Besides changes in the relative intensities of the detected elements aluminum can be detected to a distinct amount, Fig. 4b. The carbon line shape corresponds rather to graphite than to carbide, carbonate or CO adsorption. See for comparison the compilation of peak shapes of carbon in several compounds in [26].

To investigate any possible mass transport in the neighborhood of the crack, an Auger depth profile has been recorded. In *Fig. 5*, the corresponding amplitudes of the differentiated Auger lines are plotted as a function of sputter time. The inset in Fig. 5 shows the splitted aluminium KLL peak after a sputter time of 300 s. The measured shift of 6 eV between metallic and oxidized aluminium is much smaller than literature values for the chemical shift of Al_2O_3. This corresponds to a partial oxidation of Al, which is also supported by the low oxygen concentration of the order of 20% that was found from the surface on up to a sputter time of 400 s. For magnesium, no chemical shift and no peak shape modifications as a function of sputter depth have been detected. This may correspond to partially oxidized

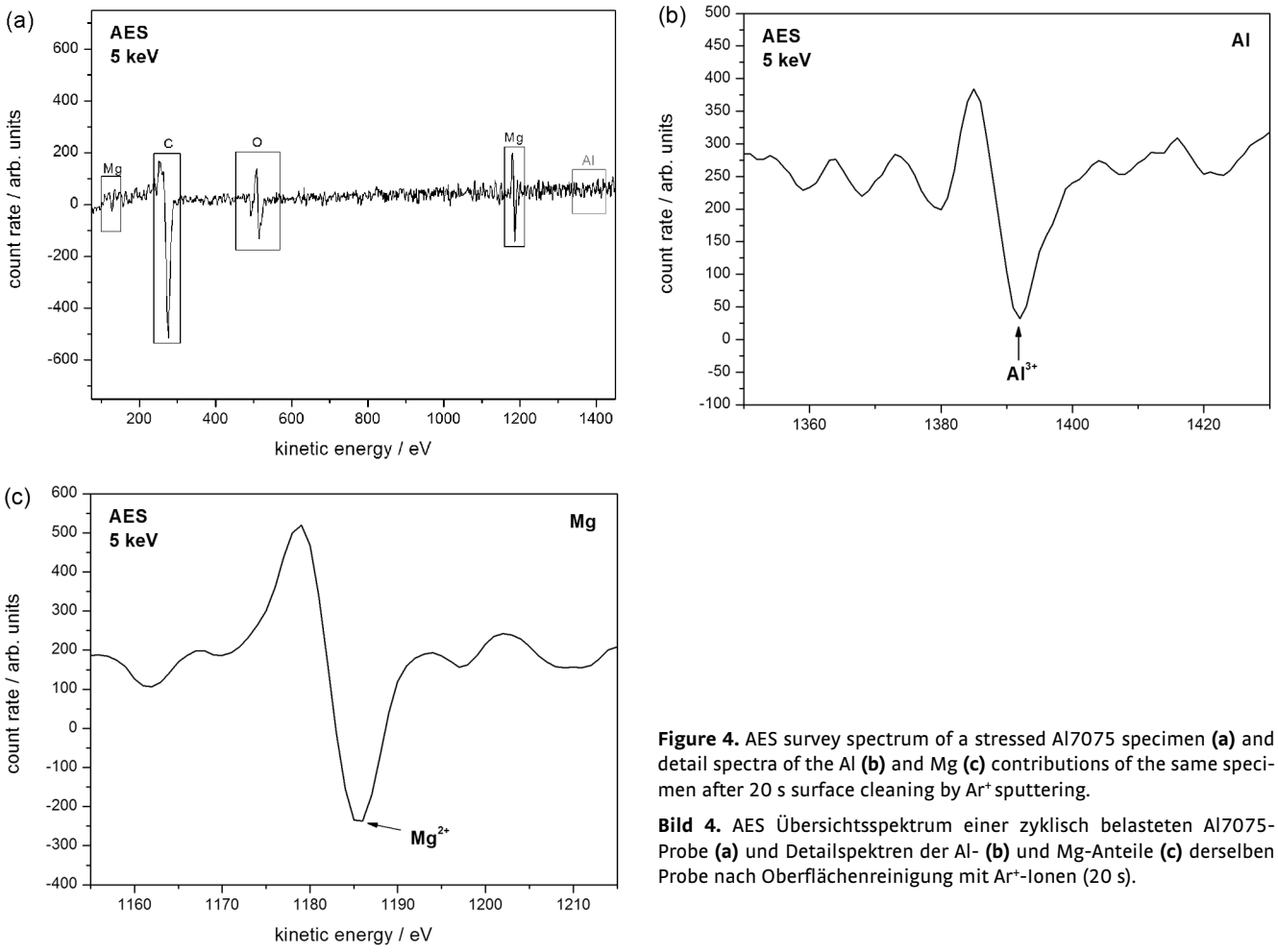

Figure 4. AES survey spectrum of a stressed Al7075 specimen **(a)** and detail spectra of the Al **(b)** and Mg **(c)** contributions of the same specimen after 20 s surface cleaning by Ar^+ sputtering.

Bild 4. AES Übersichtsspektrum einer zyklisch belasteten Al7075-Probe **(a)** und Detailspektren der Al- **(b)** und Mg-Anteile **(c)** derselben Probe nach Oberflächenreinigung mit Ar^+-Ionen (20 s).

magnesium. The concentration of magnesium exceeds that of aluminum up to a sputter time of 200 s. The oxidized aluminum reaches its maximum at 300 s and the metallic aluminum is dominant beyond 400 s. After an initial drop due to the removal of the adsorbate layer the carbon component remains on a nearly constant level before it falls off with the upcoming metallic aluminium. For the first 100 s of sputtering the carbon peak shape agrees well with that of graphite. After longer sputter times the maximum of the differentiated carbon peak splits which is typical of amorphous graphite [26]. After the removal of the partially oxidized layer the intensity is too low for a peak shape analysis.

A few SEM images for different sputter depths, show the removal of the oxidized layer with high carbon content (corresponding to the dark color) and the transition to a dominant metallic Al concentration (bright regions) by significant contrast modifications, *Fig. 6*. The spectrum in Fig. 5 was recorded at the spot marked in Fig. 6. Farther away from the crack the dark color is removed already after a few seconds sputtering. Closer to the crack a few hundred seconds are needed. A similar behavior of the depth profile has been found all along the crack in the dark-colored rim. To evaluate the extension of this zone of remarkable material transport Auger spectra have been recorded after 100 s Ar^+ sputtering at distances of about 3 mm and close to the crack, at the marked positions in *Fig. 7*. 3 mm apart from the crack, a Mg concentration of the order of 5 at.-% is found when only metallic components are considered. This is still more than the average magnesium concentration in Al7075 of about 3 at.-% but less than the maximum local magnesium concentration found at the surface of the untreated reference specimens which have only been cut and polished. After 200 s Ar^+ ion sputtering the carbon contamination vanished and only some oxygen as non-metallic constituent is detected. The concentration of the metallic components (93.8 at.-% aluminium, 3.5 at.-% magnesium and 2.7 at.-% zinc) are close to nominal bulk values.

In the dark region directly adjacent to the crack, no aluminium is detected at all, Fig. 7, position 1. The surface consists only of carbon and oxidized magnesium. In the brighter regions, the carbon contribution is less pronounced, Fig 7, position 2. The magnesium and oxygen concentration is much higher, but still no aluminium is detectable. Only farther away from the crack, aluminium can be detected, and the sample is almost free of carbon, Fig. 7, position 3. In contrast to the reference region 3 mm apart from the crack, the sample shows a significantly reduced magnesium concentration at position 3. This indicates a magnesium depletion in the intermediate region.

In summary, three different regions can be detected at the surface:

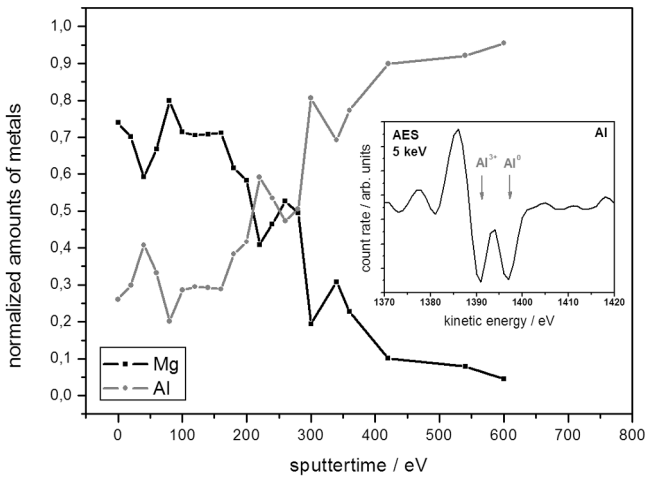

Figure 5. Depth profiles of Al and Mg for the stressed Al7075 specimen at the position marked in the SEM images in Fig. 6, the analyzed area is 145×175 nm^2, the sputter area is much larger and exceeds the image size, it amounts to about 1400×1400 μm^2, the inset shows the splitted aluminium KLL peak after a sputter time of 300 s.

Bild 5. Tiefenprofile von Al und Mg für eine zyklisch belastete Al7075-Probe, aufgezeichnet an der in Fig. 6 markierten Stelle, die analysierte Stelle ist 145×175 nm^2 groß, der gesputterte Bereich ist sehr viel größer als der dargestellte Bildbereich und beträgt etwa 1400×1400 μm^2, die Einfügung zeigt den geteilten KLL-Übergang an Aluminium nach 300 s Sputterzeit.

1. A strong magnesium enrichment at the crack with very carbon rich regions directly adjacent to the crack at positions 1 and 2.
2. An intermediate region some micrometers apart from the crack, that exhibits a magnesium depletion.
3. The region some millimeters away from the crack, where the surface shows a composition close to nominal bulk values.

Summarizing these results, this shows a segregation of the magnesium towards the crack. The affected region seems to be some micrometers wide.

4 Discussion

A significant magnesium transport from bulk to surface is found in the crack region. In SEM images this zone is highlighted by its dark color and extends up to 1000 nm to either sides of the crack. At a few 100 μm distance from the crack, the magnesium concentration at the surface drops down to values below 10 at.-% of the metals in the alloy. An increase of the magnesium concentration by a factor of up to 3 is typical of polished specimens as seen at the untreated reference specimen. Whereas in the farther surrounding the magnesium concentration drops down to bulk values after 100 to 200 s sputtering the same magnesium content is reached at an equivalent depth of more than 600 s close to the crack.

The quite high carbon concentration runs plateau like up to a sputter time of 300 s and then drops down to below the detection limit. The plateau like behavior is similar to the characteristics of the magnesium concentration. The aluminium concentration exceeds that of magnesium from 300 s on when metallic aluminium becomes dominant and the oxidized aluminum is nearly removed.

What is the nature of this modified crack zone? A simple stoichiometric oxide film can be ruled out for the first 300 s in the depth profile because of the low ($\leq$ 25 at.-%) oxygen concentration, which is within the limits of accuracy nearly constant. As

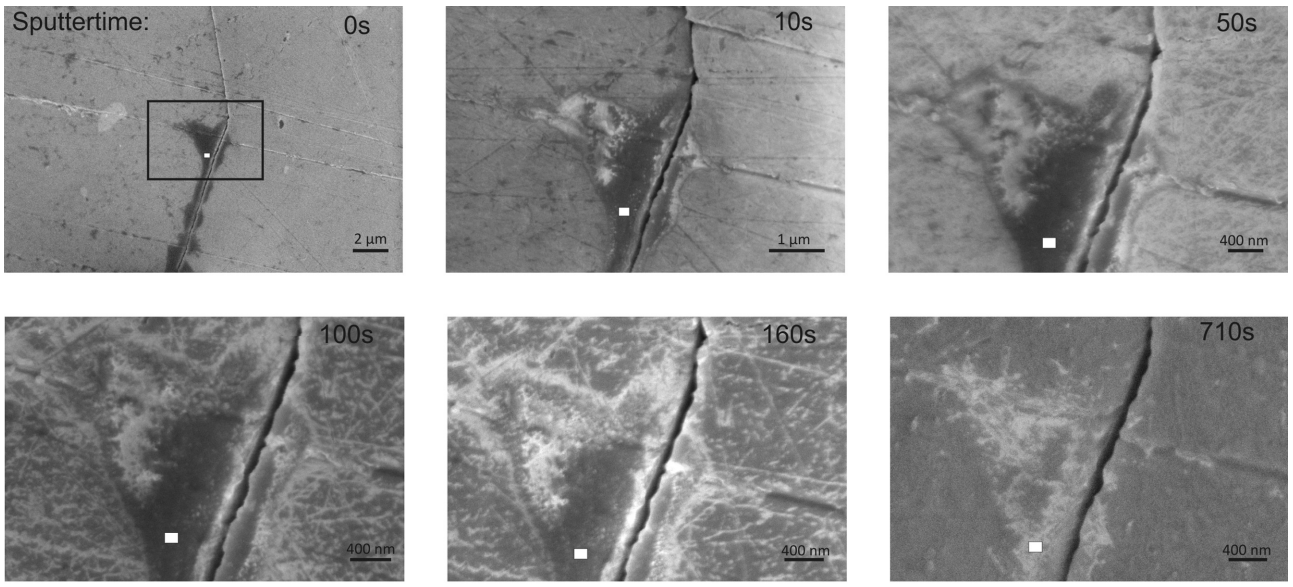

Figure 6. SEM images taken during the depth profiling, the white rectangles mark the positions where the Auger spectra are obtained as described in Fig. 5, the image sizes are given respectively.

Bild 6. Rasterelektronenmikroskopische Aufnahmen, die während der Tiefenprofileanalyse aufgezeichnet wurden, die weißen Rechtecke bezeichnen die Position an der die Augerspektren aus Fig. 5 aufgenommen wurden, die dargestellten Bildgrößen sind jeweils angezeichnet.

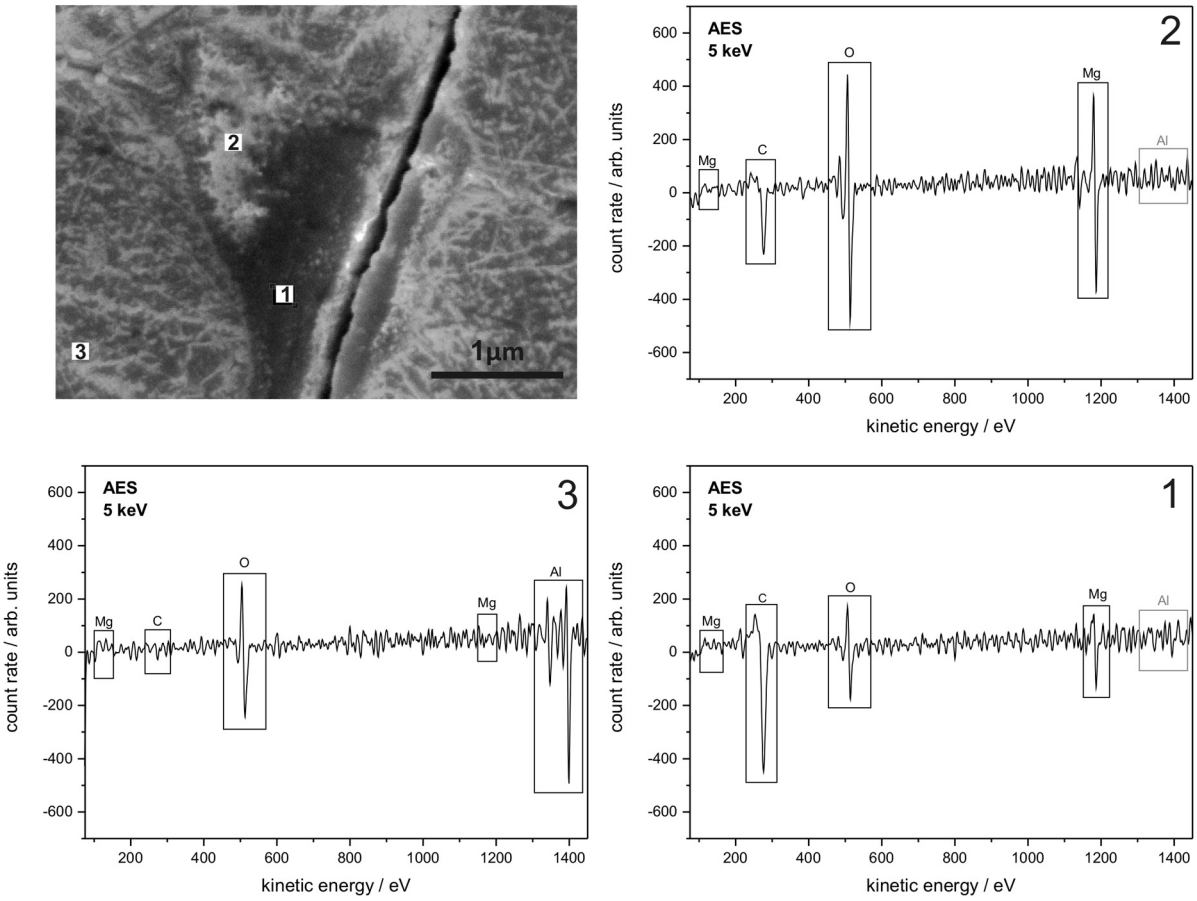

Figure 7. SEM image of the crack and the surrounding area along with Auger survey spectra of the positions (1), (2) and (3) after 100 s Ar^+ sputtering.

Bild 7. Rasterelektronemikroskopische Aufnahme des Risses und der Umgebung nach Oberflächenreinigung mit Ar^+-Ionen (100 s), zusammen mit Augerspektren, die an den Positionen (1), (2) und (3) aufgezeichnet wurden.

mentioned above, the shape of the carbon peaks fits rather to graphite than to carbonate or adsorbed CO. It is also not carbidic. Carbides are easily identifiable in AES by two well resolvable side peaks at the lower energy side. What is the origin of the carbon? Two sources may be considered: atmospheric carbon and residual carbon in Al7075. The concentration of the latter is quite small in comparison to the carbon concentration at the surface due to adsorption of atmospheric carbon. Thus, the carbon enrichment in the crack zone is considered to be due to direct adsorption from the atmosphere or due to surface transport of adsorbed carbon. In recent papers the interaction of oxygen and carbon dioxide on calcium and CaO surfaces has been investigated and a formation of CaO, Ca-C-O complexes and adventitious carbon was found [27, 28]. This is similar for many mineral-like surfaces [29]. Especially, similar results can be expected after exchanging calcium with the chemical similar magnesium. The energy input by the periodic load promotes the carbon transport deeper into the bulk. This is in particular true for the disordered crack zone.

So far the possible role of hydrogen has not been discussed. Hydrogen cannot be detected by AES. Thus, the discussion can only be held by adapting findings from other work. Song et al. discussed the role of hydrogen in fatigue of the 7050 aluminum alloy [7]. The authors pointed out that hydrogen has a higher affinity to magnesium than to aluminium. Thus, a notable amount of hydrogen might have reacted with the segregated magnesium close to the crack.

In the literature also the precipitation of the magnesium-rich β phase (Al_3Mg_2) as SCC determining effect has been reported as a result of thermal aging [6]. In our case (FCC) no such phases could be detected.

The metals (aluminium and magnesium) in the crack zone surface are partially oxidized. Throughout the whole depth that shows magnesium enrichment, graphite like carbon can be detected, which suggests a rather open structure enabling carbon agglomeration or an intercalation like structure.

What is the mechanism leading to the crack zone? It is well known, that aluminium- magnesium alloys show magnesium enrichment after annealing even at temperatures of less than 200 °C, which results in a strong magnesium enrichment at the surface [8, 9]. This is even observed on aluminium-silicon alloys, where magnesium with a concentration of 0.15 at.-% is only a minor component [9]. Since magnesium is supposed to segregate at grain boundaries at such temperatures magnesium cati-

ons obviously have a sufficient mobility probably at grain boundaries to reach the surface [7]. The fatigue load was applied at room temperature. Thus, the energy supplied by the materials deformation is obviously sufficient to mobilize the magnesium. Driving force for the enormous magnesium enrichment in the crack zone is in part the formation of magnesium oxide because the heat of formation is higher for magnesium oxide than for alumina [8, 9]. But also the formation of a carbon-magnesium complex might favor the process.

The mechanical strength of such a region with modified composition and especially a high, graphite-like carbon concentration is probably low. Thus, a crack of a few nm depth will form easily. The disordered structure of such segregated material will also favor atmospheric corrosion by an increased access of corrosive molecules below the surface in particular, because the magnesium oxide is known to be less stable in comparison to alumina [30].

5 Summary

Scanning electron microscopy has been employed to image the surfaces of Al7075 specimen before and after exposure to mechanical stress in a resonance testing apparatus. The chemical analysis of these surfaces via Auger electron spectroscopy with a lateral resolution down to 5 nm has been alterated with Ar^+ ion sputter etching cycles, thus obtaining chemical depth profiles. The unstressed specimen revealed a slight Mg enrichment induced by the mechanical treatment. The stressed specimen showed a crack with a total length of approximately 3 mm. Within a distance of up to 1 µm to either side of the crack, a severe Mg enrichment was found, where the Mg concentration even exceeds the Al concentration by far.

The depth of the Mg concentration layer has been determined to amount to at least 19 nm according to sputter rate for the Al_2O_3 reference. The concentration layer was found to be partially oxidized, thus suggesting the concentration gradient due to the oxidation reaction might possibly be the driving force of the Mg diffusion towards the surface. Nevertheless, the repeated mechanical stress from the cyclic load must be strongly enhancing the magnesium atoms mobility and thus be the origin of the diffusion rate required for the described segregation effect.

Acknowledgement

The authors gratefully acknowledge Dipl.-Ing. Fabian Pönisch for the FEM calculations and the support by Dipl.-Ing. Timothy Mark Medhurst.

6 References

[1] P. J. E. Forsyth, *The physical basis of metal fatigue*, Blackie and Son, London **1969**.
[2] J. Schijve, *International Journal of Fatigue* **2003**, *25*, 679.
[3] J. Schijve, Fatigue of Structures and Materials, Springer, **2009**.
[4] G. Hénaff, G. Odemer, A. Tonneau-Morel, *International Journal of Fatigue* **2007**, *29*, 1927.
[5] W. T. Becker, Principles of failure analysis – fatigue failures, course 0335 lesson 4, ASM International **2002**.
[6] R. H. Jones, D. R. Baer, M. J. Danielson, J. S. Vetrano, *Met. Mat. Trans. A* **2001**, *32*, 1699.
[7] R. G. Song, M. K. Tseng, B. J. Zhang, J. Liu, Z. H. Jin, K. S. Shin, *Acta Mater.* **1996**, *44*, 3241.
[8] G. R. Wakefield, R. M. Sharp, *Appl. Surf. Sci.* **1991**, *51*, 95.
[9] C. R. Werrett, D. R. Pyke, A. K. Bhattacharya, *Sur. Int. Anal.* **1997**, *25*, 809.
[10] S. Zhang, O. Y. Kontsevoi, A. J. Freeman, G. B. Olson, *Appl. Phys. Lett.* **2012**, *100*, 231904.
[11] J. M. Chen, T. S. Sun, R. K. Viswanadham, J. A. S. Green, *Metall. Trans. A* **1977**, *8*, 1935.
[12] W. Gruhl, *Z. Metallk.* **1984**, *75*, 819.
[13] S. L. Cundy, A. J. F. Metherel, M. J. Whelan, P. N. T. Unwin, R. B. Nicholson, *Proc. R. Soc. London A* **1968**, *307*, 267.
[14] P. Doig, J. W. Edington, *Metall. Trans. A* **1975**, *6*, 943.
[15] C. R. Shastry, G. Judd, *Metall. Trans.* **1972**, *3*, 779.
[16] R. H. Jones, D. R. Baer, M. J. Danielson, J. S. Vetrano, *Metall. Trans. A* **2001**, *32*, 1699.
[17] J. R. Pickens, T. J. Langan, *Metall. Trans. A* **1987**, *18*, 1735.
[18] G. Ertl, J. Küppers, *Low energy electrons and surface chemistry*, VCH Verlagsgesellschaft, **1985**.
[19] I. F. Ferguson, *Auger Microprobe Analysis*, IOP Publishing Ltd., Bristol, New York **1989**.
[20] http://www.capalex.co.uk/german/7075_alloy_ge.html.
[21] R. Blümke, C. Müller, *Materialwiss. u. Werkstofftech.* **2002**, *33*, 520.
[22] http://www.omicron.de/en/products/nanoprobing-nano sam-lab/instrument-concept.
[23] Th. Wagner, J.Y. Wang, S. Hoffmann in D. Briggs, J.T. Grant (eds.), *Surface Analysis by Auger and X-ray Photoelectron Spectroscopy*, IM Publications, Chichester **2003**, 619 ff.
[24] D. R. Baer, M. H. Engelhard, A. S. Lea, P. Nachimuthu, T. C. Droubay, J. Kim, B. Lee, C. Mathews, R. L. Opila, L. V. Saraf, W. F. Stickle, R. M. Wallace, B. S. Wright, *J. Vac. Sci. Technol. A* **2010**, *28*, 1060.
[25] M. Frerichs, F. Voigts, W. Maus-Friedrichs, *Appl. Surf. Sci.* **2006**, *253*, 950.
[26] I.F. Ferguson, Auger Micro Probe Analysis, Adam Hilger IOP Publishing Ltd., Bristol, New York **1989**, chapter 4.
[27] F. Bebensee, F. Voigts, W. Maus-Friedrichs, *Surf. Sci.* **2008**, *602*, 1622.
[28] F. Voigts, F. Bebensee, S. Dahle, K. Volgmann, W. Maus-Friedrichs, *Surf. Sci.* **2009**, *603*, 40.
[29] P. van Capellen, L. Charlet, W. Stumm, P. Wersin, *Geochim. Cosmochim. Acta* **1993**, *57*, 3505.
[30] D. R. Lide, *CRC Handbook of Chemistry and Physics*, CRC Press LLC, **1998**, ISBN 0-8493-0479-2.

Received on final form: March 21st 2013 T 52

